Statistical properties of light from optical parametric oscillators

Reeta Vyas and Surendra Singh
Department of Physics, University of Arkansas, Fayetteville, Arkansas 72701, USA
(Received 6 October 2009; published 16 December 2009)

Coherence properties of light beams generated by optical parametric oscillators (OPOs) are discussed in the region of threshold. Analytic expressions, that are valid throughout the threshold region, for experimentally measurable quantities such as the mean and variance of photon number fluctuations, squeezing of field quadratures, and photon counting distributions are derived. These expressions describe non-Gaussian fluctuations of light in the region of threshold and reproduce Gaussian fluctuations below and above threshold, thus providing a bridge between below and above threshold regimes of operation. They are used to study the transformation of fluctuation properties of light as the OPOs make a transition from below to above threshold. The results for the OPOs are compared to those for the single-mode and two-mode lasers and their similarities and differences are discussed.

DOI: 10.1103/PhysRevA.80.063836 PACS number(s): 42.50.Ar, 42.65.Yj, 42.65.Lm, 42.50.Lc

I. INTRODUCTION

Nonclassical properties of light have continued to draw considerable attention both from conceptual and practical viewpoints [1]. Perhaps the most important sources of light where nonclassical features of light have been studied recently are optical parametric oscillators (OPOs) based on frequency down conversion [2–12]. In optical frequency down conversion, a pump photon at frequency ω_3 is converted into two photons of lower frequencies ω_1 and ω_2 $(\omega_3=\omega_1+\omega_2)$. The oscillator is termed degenerate optical parametric oscillator (DPO) if the down-converted photons have the same frequency, momentum, and polarization, otherwise it is called nondegenerate optical parametric oscillator (NDPO). In an OPO, frequency down conversion occurs inside an optical cavity whereas in an optical parametric amplifier (OPA), it occurs outside a cavity. Nonclassical character of light produced by parametric oscillators is reflected in field quadrature squeezing, sub-Poissonian statistics, and antibunching of photons in certain interference (homodyne or heterodyne) experiments when the relative phase of interfering beams is varied [2,9,10]. In addition to these familiar signatures, down-converted photons may also be entangled nonclassically in polarization, frequency, momentum, and phase. This means these properties of down-converted photons are strongly correlated in a way that can only be described quantum mechanically.

Nonclassical signatures of light from OPOs have been studied experimentally as well. However, with few exceptions [3–6], these experiments have been carried out on OPAs or OPOs operating below threshold. In this regime, the state of the light is well approximated by a Gaussian (as described by Wigner function or the positive-P function) and this has formed a reasonably good basis for understanding nonclassical photon statistics and entanglement below threshold [13–15].

In crossing the threshold, the system makes a transition from an amplifier (with or without filter cavity) to an oscillator resulting in profound changes in its behavior. Near threshold, the state of light from an OPO is non-Gaussian and photon statistics of the OPOs in this regime have remained largely unexplored. In many ways, the threshold transition in OPOs is expected to be laserlike [16,17]. However, because of phase sensitive and multiplicative nature of quantum noise in OPO, significant differences are also to be expected. Indeed, we find that while the DPO photon number distribution above threshold is similar to a laser, it still exhibits squeezing [18]. Similarly, while each mode of a NDPO individually may behave like a laser, the two modes stay entangled. Consequently, an interference between the two beams at a beam splitter [19,20] may create a nonclassical squeezing of photon number difference and or relative phase difference in accordance with the number-phase Heisenberg uncertainty [21].

Positive-P representation [22] has played important role in elucidating the quantum nature of light from the OPOs. The advantage of positive-P distribution is that it has all the features of a probability density and allows quantum dynamics of the OPOs to be mapped onto a classical stochastic process [13,14,18,23–25]. Using this approach, the fluctuation properties of light generated by the OPOs below and above threshold have been studied in terms of Gaussian random variables [25–30]. This is possible because the equations of motion can be linearized around the steady state far and above threshold. Near threshold, where a linearized treatment is not valid, the spectrum of squeezing [31] and the positive-P distribution for the DPO have also been calculated [13,14,18,23]. The NDPO has also been discussed by using a generalized P representation of the density matrix [32]. However, although the generalized P function itself could be obtained in a closed form, it was not possible to derive analytic expressions for other quantities of interest in terms of tabulated functions.

In this paper, we use the positive-P distribution to study the transformation of fluctuations of light analytically as the operating point of the OPO crosses threshold. We derive simple expressions for the positive-P function near threshold and use it to obtain analytic expressions for many experimentally measurable quantities. These expressions remain valid throughout the threshold region and provide a unified description of the transformation of fluctuations of light in passing the threshold. In Sec. II, we consider the fluctuation properties of a DPO and compare and contrast them to a single-mode laser. In Sec. III, we consider a NDPO and compare and contrast its fluctuation properties to two-mode la-

sers. The paper ends with a summary of the principal conclusions of the paper.

II. DEGENERATE PARAMETRIC OSCILLATOR

In a degenerate parametric oscillator, a nonlinear crystal is placed inside an optical cavity, which is excited by a classical field of frequency 2ω with dimensionless amplitude ε normalized such that $|\varepsilon|^2$ is the number of pump photons entering the cavity in one cavity lifetime $(2\gamma_3)^{-1}$ at the pump frequency. Inside the cavity, the nonlinear crystal down-converts a pump photon into two photons of frequency ω. Hamiltonian for the system can be written as

$$\hat{H} = \frac{1}{2} i\kappa(\hat{a}^{\dagger 2}\hat{a}_3 - \hat{a}^2\hat{a}_3^\dagger) + i\hbar\gamma_3\varepsilon(\hat{a}_3^\dagger - \hat{a}_3) + \hat{H}_{loss}, \quad (1)$$

where κ is the mode coupling constant, which can be expressed in terms of the second-order nonlinear susceptibility of the crystal and certain integrals over mode functions, $\hat{a}_3$ and $\hat{a}_3^\dagger$ are the annihilation and creation operators for the pump mode, $\hat{a}$ and $\hat{a}^\dagger$ are annihilation and creation operators for the subharmonic (down-converted) mode, and $\hat{H}_{loss}$ describes mode losses due to scattering, absorption, mirror transmission, and other mechanisms. If the cavity lifetime $(2\gamma_3)^{-1}$ at pump frequency is short compared to the cavity lifetime $(2\gamma)^{-1}$ at subharmonic frequency $(\gamma_3 \gg \gamma)$, the pump mode $\hat{a}_3$ can be adiabatically eliminated. Then the density matrix $\hat{\rho}$ for the subharmonic field can be expressed in terms of the phase-space density $\mathcal{P}$ in the positive-P representation as [22]

$$\hat{\rho} = \int\int_{\mathcal{D}} d^2\alpha d^2\alpha_* \frac{|\alpha\rangle\langle\alpha_*|}{\langle\alpha_*|\alpha\rangle}\mathcal{P}(\alpha,\alpha_*), \quad (2)$$

where $\mathcal{D}$ is a suitably chosen domain in the four-dimensional phase space spanned by the complex variables α and α_* such that $\mathcal{P}(\alpha,\alpha_*)$ is real, positive, and normalized to unity. Complex variables α and α_* are associated with the operators $\hat{a}$ and $\hat{a}^\dagger$ via $\hat{a}|\alpha\rangle = \alpha|\alpha\rangle$ and $\langle\alpha_*|\hat{a}^\dagger = \alpha_*\langle\alpha_*|$. In the positive-$P$ representation, α and α_* are not complex conjugates of each other. The positive-P distribution satisfies the Fokker-Planck equation [13,14]

$$\begin{aligned}\frac{\partial\mathcal{P}(\alpha,\alpha_*)}{\partial\tau} &= -\frac{\partial}{\partial\alpha}\left[-\alpha + \frac{1}{n_o}(\sigma-\alpha^2)\alpha_*\right]\mathcal{P}(\alpha,\alpha_*) \\ &+ \frac{1}{2n_o}\frac{\partial^2}{\partial\alpha^2}\sqrt{\sigma-\alpha^2}\mathcal{P}(\alpha,\alpha_*) - \frac{\partial}{\partial\alpha_*}\left[-\alpha_*\right. \\ &\left. + \frac{1}{n_o}(\sigma-\alpha_*^2)\alpha\right]\mathcal{P}(\alpha,\alpha_*) + \frac{1}{2n_o}\frac{\partial^2}{\partial\alpha_*^2}\sqrt{\sigma-\alpha_*^2}\mathcal{P}(\alpha,\alpha_*). \quad (3)\end{aligned}$$

Here, $\tau = \gamma t$ is dimensionless time [cavity lifetime being $(2\gamma)^{-1}$], $\sigma = 2\gamma_3\varepsilon/\kappa$ is scaled pump field amplitude, and $n_o = 2\gamma\gamma_3/\kappa^2$ is a number, which will be seen to be of the order of the square of the mean number of photons in the cavity at threshold. Threshold of the DPO is defined by $\sigma/n_o \equiv \kappa\epsilon/\gamma = 1$. Note that the ratio $\kappa\epsilon/\gamma$ is essentially the ratio of linear gain to loss at the subharmonic frequency.

The form of the diffusion terms in the Fokker-Planck equation suggests that if α and α_* are real initially, they remain so for all times. Since the DPO starts out in the vacuum state initially, which satisfies this criterion, the system dynamics is confined to the subspaces $\alpha = x_1$ and $\alpha_* = x_2$, where x_1 and x_2 are real variables. In this manifold, the steady-state positive-P distribution function can be written as [13,14]

$$\mathcal{P}(x_1,x_2) = \text{const}[(\sigma - x_1^2)(\sigma - x_2^2)]^{n_o - 1}\exp[2x_1x_2] \quad (4)$$

where $|x_1|, |x_2| \le \sqrt{\sigma}$. From this positive-$P$ function, we can calculate the steady-state fluctuation properties of the DPO. In particular, the normally ordered operator averages can be computed according to the correspondence

$$\langle :\hat{a}^{\dagger m}\hat{a}^n: \rangle \to \int\int dx_1 dx_2 x_2^m x_1^n \mathcal{P}(x_1,x_2). \quad (5)$$

The distribution in Eq. (4) can be simplified by noting that the parameter n_o is a large number of the order of $\approx 10^6 - 10^8$ for most laboratory systems. This means the distribution $\mathcal{P}(x_1,x_2)$ is essentially zero well before the boundary $|x_1|, |x_2| < \sqrt{\sigma}$ is reached. In this case, it is more convenient to introduce scaled variables

$$u_1 = \left(\frac{n_o}{8\sigma^2}\right)^{1/4}(x_1 + x_2) \quad \text{and} \quad u_2 = \left(\frac{n_o}{8\sigma^2}\right)^{1/4}(x_1 - x_2). \quad (6)$$

These variables may be thought of as scaled pseudoquadrature variables. In terms of these variables, the steady-state distribution can be written to an excellent approximation as

$$\mathcal{P}(u_1,u_2) \approx \frac{1}{N}\exp\left[a_1u_1^2 + a_2u_2^2 - \frac{1}{2}(u_1^4 + u_2^4 + 6u_1^2u_2^2)\right], \quad (7)$$

where N is a normalization constant and a_1 and a_2 are dimensionless parameters given by

$$a_1 = (\sigma/n_o - 1)\sqrt{2n_o} = (\kappa\varepsilon/\gamma - 1)\sqrt{2n_o}, \quad (8)$$

$$a_2 = -(\sigma/n_o + 1)\sqrt{2n_o} = -(\kappa\varepsilon/\gamma + 1)\sqrt{2n_o}. \quad (9)$$

These parameters depend on the ratio of gain to loss $\kappa\epsilon/\gamma$ and are analogous to the pump parameter of the conventional single-mode laser theory [16]. Using the normalization condition $\int\int_{-\infty}^{\infty}\mathcal{P}(u_1,u_2)du_1du_2 = 1$, we find that the normalization constant N is given by

$$N = \sqrt{\pi}\int_0^\infty ds\ \ s^{-1/2}\exp\left[a_1s - \frac{1}{2}s^2 + \frac{1}{4}(3s + |a_2|)^2\right] \times D_{-1/2}(3s + |a_2|), \quad (10)$$

where $D_\nu(z)$ is parabolic cylinder function of order ν and argument z given by [33]

$$D_\nu(z) = \frac{\exp(-z^2/4)}{\Gamma(-\nu)}\int_0^\infty dt\ \ t^{-\nu-1}\ \exp\left[-\left(\tfrac{1}{2}t^2 + zt\right)\right], \quad \nu < 0 \quad (11)$$

and $\Gamma(x)$ is Gamma function of argument x. We will find the following limiting forms of $D_\nu(z)$ for real z useful for the discussion in the paper:

$$D_\nu(z) = \begin{cases} e^{-(1/4)z^2} z^\nu \left[1 - \dfrac{\nu(\nu-1)}{2z^2} + \cdots \right], & z > 0, \ |z| \gg 1, |\nu| \\ \dfrac{e^{(1/4)z^2}\sqrt{2\pi}}{|z|^{\nu+1}\Gamma(-\nu)} \left[1 + \dfrac{(\nu+1)(\nu+2)}{2z^2} + \cdots \right], & z < 0, \ |z| \gg 1, |\nu|. \end{cases} \tag{12}$$

The steady-state distribution (7) is an even function of both u_1 and u_2 as it depends only on u_1^2 and u_2^2. This means only the averages involving even powers of u_1 and u_2 will give nonzero results. The steady-state distribution $\mathcal{P}(u_1,u_2)$ is similar to the distribution for two strongly coupled laser modes with pump parameters a_1 and a_2, provided u_1^2 and u_2^2 are treated as mode intensities [34,35]. This observation serves as a useful guide to the approximations that can be used to obtain simple expressions for various physically observable quantities.

A. Field quadrature squeezing

From the steady-state distribution, we can compute normally ordered averages of physical quantities once they are expressed in terms of u_1 and u_2. Thus normally ordered variances of field quadratures $\hat{X} \equiv (\hat{a}+\hat{a}^\dagger)/2$ and $\hat{P} \equiv (\hat{a}-\hat{a}^\dagger)/2i$ will be given by

$$\langle :(\Delta\hat{X})^2: \rangle = \sqrt{\frac{\sigma^2}{2n_o}} \langle u_1^2 \rangle, \tag{13}$$

$$\langle :(\Delta\hat{P})^2: \rangle = -\sqrt{\frac{\sigma^2}{2n_o}} \langle u_2^2 \rangle, \tag{14}$$

where the quadrature fluctuations $\Delta\hat{X} \equiv \hat{X} - \langle\hat{X}\rangle$, $\Delta\hat{P} \equiv \hat{P} - \langle\hat{X}\rangle$ and we have used the fact that the average values of both quadrature amplitudes vanish in the steady-state since $\langle u_1 \rangle = 0 = \langle u_2 \rangle$. From these equations, we immediately see that the normally ordered variance of $\hat{X}$ is positive whereas that of $\hat{P}$ is negative. For classical fields, these variances are always positive. Negative value of normally ordered variance of quadrature $\hat{P}$ implies squeezing of its fluctuations indicating their nonclassical character. It is clear that u_1 corresponds to unsqueezed field quadrature and u_2 corresponds to squeezed field quadrature.

Averages such as Eqs. (13) and (14) can be calculated from the joint distribution $\mathcal{P}(u_1,u_2)$ directly or from the distributions $\mathcal{P}_1(u_1)$ and $\mathcal{P}_2(u_2)$, which are obtained by integrating the joint distribution $\mathcal{P}(u_1,u_2)$ with respect to u_2 and u_1, respectively. This leads to the following expressions for $\mathcal{P}_1(u_1)$ and $\mathcal{P}_2(u_2)$ which are valid throughout the threshold region:

$$\mathcal{P}_1(u_1) = \frac{\sqrt{\pi}}{N} \exp(a_1 u_1^2 - u_1^4/2) \exp[(3u_1^2 - a_2)^2/4] \times D_{-1/2}(3u_1^2 - a_2), \tag{15}$$

$$\mathcal{P}_2(u_2) = \frac{\sqrt{\pi}}{N} \exp(a_2 u_2^2 - u_2^4/2) \exp[(3u_2^2 - a_1)^2/4] \times D_{-1/2}(3u_2^2 - a_1). \tag{16}$$

These can be simplified further by noting the following. From the definition (8) of pump parameter a_1, we see that it changes from negative below threshold to positive above threshold and vanishes at threshold $\kappa\epsilon/\gamma = 1$. Therefore, the distribution for u_1 is centered at zero below threshold and at $u_1 \approx \pm\sqrt{a_1}$ above threshold. In contrast, the parameter a_2 defined by Eq. (9) is always a large negative number and its magnitude increases as a_1 increases from below to above threshold. Indeed, near threshold $\kappa\epsilon/\gamma \approx 1$, this parameter $a_2 \approx -\sqrt{8n_o}$, which for a typical value $n_o \approx 10^6$ gives $|a_2| \approx 3 \times 10^3 \gg 1$. Thus the argument $3u_1^2 - a_2 = 3u_1^2 + |a_2|$ of parabolic cylinder function in Eq. (15) is a large positive number for all values of u_1. In light of these observations, we can use the asymptotic form (12) of $D_{-1/2}$ for large positive arguments and write the distribution for u_1 as

$$\mathcal{P}_1(u_1) = \frac{1}{\sqrt{\pi}} \frac{\exp\left(-\frac{1}{4}a_1^2\right)}{D_{-1/2}(-a_1)} \exp\left(a_1 u_1^2 - \tfrac{1}{2}u_1^4\right). \tag{17}$$

This expression holds in the threshold region from below to above threshold. Similar considerations for $\mathcal{P}_2(u_2)$ show that, since a_2 is a large negative number, the distribution for u_2 remains centered at zero. Its width, however, depends on a_1. This is because the parabolic cylinder function has different asymptotic limits for large positive and large negative values of its argument $3u_2^2 - a_1$, which can take large positive values below threshold ($a_1 < 0$) and large negative values above threshold ($a_1 > 0$). Using the asymptotic form for D_ν far below and above threshold, we find that $\mathcal{P}_2(u_2)$ can be written as

$$\mathcal{P}_2(u_2) = \sqrt{\frac{1}{2\pi\langle u_2^2 \rangle}} \exp(-u_2^2/2\langle u_2^2 \rangle) \tag{18}$$

$$\langle u_2^2 \rangle = \begin{cases} \dfrac{1}{2|a_2|}, & \text{below threshold } (a_1 < 0) \\ \dfrac{1}{2(3a_1 + |a_2|)}, & \text{above threshold } (a_1 > 0). \end{cases} \tag{19}$$

With the help of distributions (17) and (18), we find that the moments of u_1 and u_2 are given by

$$\langle u_1^{2n} \rangle = (2n-1)!! \frac{D_{-(n+1/2)}(-a_1)}{2^n D_{-1/2}(-a_1)}, \quad \langle u_1^{2n+1} \rangle = 0, \tag{20}$$

$$\langle u_2^{2n}\rangle = (2n-1)!\,!\,\langle u_2^2\rangle^n, \quad \langle u_2^{2n+1}\rangle = 0. \tag{21}$$

Using these results in Eqs. (13) and (14), we can express the normally ordered quadrature variances as

$$\langle :(\Delta\hat{X})^2:\rangle = \sqrt{\frac{\sigma^2}{2n_o}}\frac{D_{-3/2}(-a_1)}{2D_{-1/2}(-a_1)}, \tag{22}$$

$$\langle :(\Delta\hat{P})^2:\rangle = -\sqrt{\frac{\sigma^2}{2n_o}}\langle u_2^2\rangle. \tag{23}$$

As a quick check, far below threshold ($a_1<0$, $|a_1|\gg 1$), these expressions reduce to

$$\langle :(\Delta\hat{X})^2:\rangle \to \sqrt{\frac{\sigma^2}{2n_o}}\frac{1}{2|a_1|} = \frac{1}{4}\left(\frac{\kappa\epsilon/\gamma}{1-\kappa\epsilon/\gamma}\right), \tag{24}$$

$$\langle :(\Delta\hat{P})^2:\rangle \to -\sqrt{\frac{\sigma^2}{2n_o}}\frac{1}{2|a_2|} = -\frac{1}{4}\left(\frac{\kappa\epsilon/\gamma}{1+\kappa\epsilon/\gamma}\right), \tag{25}$$

which agree with the expressions for below threshold operation [36]. From Eq. (25), we see that maximum squeezing of quadrature $\hat{P}$ occurs near threshold ($a_1=0$ or $\sigma/n_o=\kappa\epsilon/\gamma=1$). A more accurate evaluation of quadrature squeezing using Eq. (7), which can be expressed in closed form, yields a minimum slightly above threshold, the correction being of order $1/|a_2|$. Note that Eqs. (24) and (25) were derived by assuming a_1 and a_2 to be large negative numbers. This means Eq. (25) remains valid even near threshold, whereas Eq. (24) breaks down near threshold. This is because a_2 is always a large negative number whereas a_1 is a large negative number only far below threshold but vanishes as threshold is approached. Near threshold ($a_1\approx 0$ or $\sigma/n_o=\kappa\epsilon/\gamma\approx 1$), we can use the behavior of parabolic cylinder function for small arguments in Eq. (22) to arrive at the following expression for the variance of the unsqueezed quadrature:

$$\begin{aligned}\langle :(\Delta\hat{X})^2:\rangle &\approx \frac{\sigma}{n_o}\sqrt{n_o}\frac{\Gamma(3/4)}{\Gamma(1/4)}\left\{1+a_1\frac{\Gamma(1/4)}{2\sqrt{2}\Gamma(3/4)}\left[1-4\left(\frac{\Gamma(3/4)}{\Gamma(1/4)}\right)^2\right]\right\}\\ &= \frac{\sigma}{n_o}\sqrt{n_o}0.338(1+0.568a_1).\end{aligned} \tag{26}$$

This expression shows that while the fluctuations of unsqueezed quadrature continue to increase in passing the threshold, they stay finite being of order $\sqrt{n_o}/3$ near threshold. Figures 1(a) and 2(b) show the variation of normally ordered quadrature variances near threshold as functions of pump parameter a_1 which is in agreement with these conclusions.

High above threshold $a_1\gg 1$, we find

$$\langle :(\Delta\hat{X})^2:\rangle \to \sqrt{\frac{\sigma^2}{2n_o}}a_1, \tag{27}$$

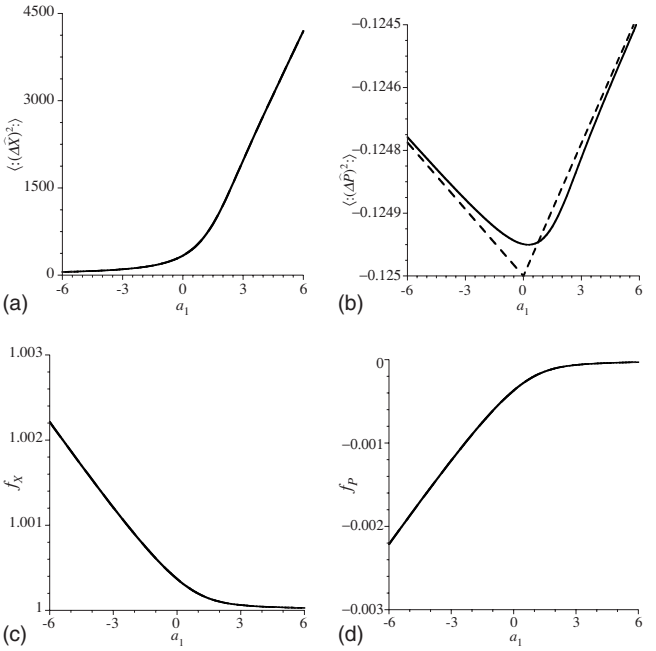

FIG. 1. [(a) and (b)] Variation of normally ordered quadrature variances $\langle :(\Delta\hat{X})^2:\rangle$ and $\langle :(\Delta\hat{P})^2:\rangle$ and [(c) and (d)] normalized quadrature variances f_X and f_P with pump parameter a_1 near threshold for $n_o=10^6$. Solid and dashed curves are obtained by using Eqs. (15) and (16) and Eqs. (17) and (18), respectively. For (a), (c), and (d), solid and dashed curves are indistinguishable. Negative values of $\langle :(\Delta\hat{X})^2:\rangle$ or $\langle :(\Delta\hat{P})^2:\rangle$ or values of f_X and f_P outside the range $0<f_X,f_P<1$ are signatures of nonclassical fields.

$$\langle :(\Delta\hat{P})^2:\rangle \to -\sqrt{\frac{\sigma^2}{2n_o}}\frac{1}{2(3a_1+|a_2|)} = -\frac{1}{8}\left(\frac{\kappa\epsilon/\gamma}{2(\kappa\epsilon/\gamma)-1}\right). \tag{28}$$

From Eq. (28), we see that with increasing pump parameter a_1, squeezing of $\hat{P}$-quadrature fluctuations decreases reaching the limit $\langle :(\Delta\hat{P})^2:\rangle \to -\frac{1}{16}$ for $a_1\gg 1$ ($\sigma/n_o=\kappa\epsilon/\gamma\gg 1$).

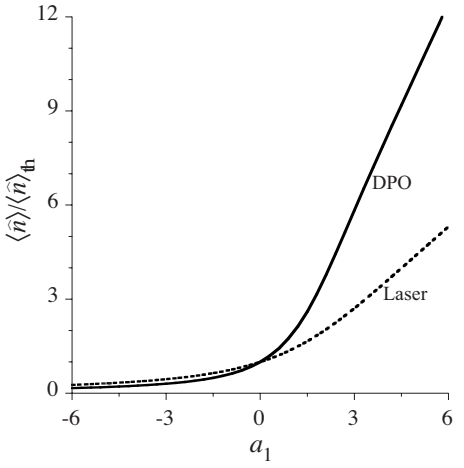

FIG. 2. Variation of mean photon number as a function of pump parameter a_1 for $n_0=10^6$. For comparison, the (dashed) curve shows the mean photon number for the single-mode laser.

This limit is approached very slowly and lies outside the pump parameter range covered by Fig. 1.

Nonclassical nature of quadrature fluctuations can also be characterized in terms of normalized variances $f_X = \langle :(\Delta\hat{X})^2: \rangle / \langle :\Delta\hat{a}^\dagger \Delta\hat{a}: \rangle$ and $f_P = \langle :(\Delta\hat{P})^2: \rangle / \langle :\Delta\hat{a}^\dagger \Delta\hat{a}: \rangle$, which for a classical fields are constrained by the inequalities [28]

$$0 \leq f_X, f_P \leq 1. \tag{29}$$

This means f_X and f_P are bounded by 0 and 1. By expressing the normalized fluctuations f_X and f_P in terms of u_1 and u_2 as

$$f_X = \frac{\langle u_1^2 \rangle}{\langle u_1^2 \rangle - \langle u_2^2 \rangle}, \quad f_P = -\frac{\langle u_2^2 \rangle}{\langle u_1^2 \rangle - \langle u_2^2 \rangle} \tag{30}$$

and using Eqs. (22) and (23), we see that for the degenerate parametric oscillator $f_X > 1$ and $f_P < 0$. Variation of f_X and f_Y with pump parameter a_1 is shown in Fig. 1. We see that f_X stays above the classical limit 1 for all pump parameter values and approaches it from above as the pump parameter increases high above threshold. Normalized fluctuations f_P of squeezed quadrature, on the other hand, are always negative, implying nonclassical nature of these fluctuations. Thus normalized fluctuations of both quadratures violate classical bounds. Characterization of quadrature fluctuations in terms of f_X and f_P brings out the nonclassical character of not only squeezed quadrature fluctuations but also unsqueezed quadrature fluctuations.

B. Photon number fluctuations

Other quantities of practical interest are the mean photon number $\langle \hat{n} \rangle$ and normalized second moment $g^{(2)}(0)$ of photon number operator. The latter is related to the normally ordered relative variance of photon number by $\langle :(\Delta\hat{n})^2: \rangle / \langle \hat{n} \rangle^2 = g^{(0)}(0) - 1$, where $\Delta\hat{n} = \hat{n} - \langle \hat{n} \rangle$ represents the deviation of photon number from its mean. The mean and normalized second moment of photon number operator can be expressed in terms of moments of u_1 and u_2 as

$$\langle \hat{n} \rangle \equiv \langle \hat{a}^\dagger \hat{a} \rangle \to \langle x_2 x_1 \rangle = \sqrt{\frac{\sigma^2}{2n_o}} \langle u_1^2 - u_2^2 \rangle, \tag{31}$$

$$g^{(2)}(0) \equiv \frac{\langle :\hat{n}^2: \rangle}{\langle \hat{n} \rangle^2} \to \frac{\langle x_2^2 x_1^2 \rangle}{\langle x_2 x_1 \rangle^2} = \frac{\langle (u_1^2 - u_2^2)^2 \rangle}{\langle u_1^2 - u_2^2 \rangle^2}. \tag{32}$$

With the help of Eqs. (20) and (21), the moments of u_1 and u_2 needed in these equations can be evaluated as

$$\langle u_1^2 - u_2^2 \rangle = \left[\frac{D_{-3/2}(a_1)}{2D_{-1/2}(a_1)} - \langle u_2^2 \rangle \right], \tag{33}$$

$$\langle (u_1^2 - u_2^2)^2 \rangle = \left[\frac{3D_{-5/2}(-a_1)}{4D_{-1/2}(-a_1)} - \frac{D_{-3/2}(-a_1)}{2D_{-1/2}(-a_1)} \langle u_2^2 \rangle + 3\langle u_2^2 \rangle^2 \right]. \tag{34}$$

Below threshold, for large negative pump parameter values, say, $a_1 < -10$, we can use the asymptotic form (12) of parabolic cylinder function and arrive at the following expressions:

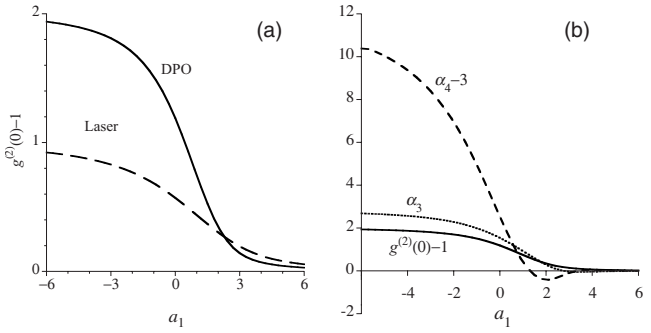

FIG. 3. Variation of normalized second-, third-, and fourth-order moments of photon number fluctuations with pump parameter a_1 for $n_0 = 10^6$. Dashed curve in (a) shows $g^{(2)}(0) - 1$ for the single-mode laser.

$$\langle \hat{n} \rangle \to \sqrt{\frac{\sigma^2}{2n_o}} \left[\frac{1}{2|a_1|} - \frac{1}{2|a_2|} \right], \tag{35}$$

$$g^{(2)}(0) \to 3 + \frac{1}{2\langle \hat{n} \rangle}. \tag{36}$$

Above threshold for large pump parameters, say, $a_1 > 10$, we find

$$\langle \hat{n} \rangle \to \sqrt{\frac{\sigma^2}{2n_o}} \left[a_1 - \frac{1}{2a_1} - \frac{1}{2(3a_1 + |a_2|)} \right], \tag{37}$$

$$g^{(2)}(0) \to 1 + \frac{1}{a_1^2} + \frac{1}{2a_1(3a_1 + |a_2|)}. \tag{38}$$

At threshold $a_1 = 0$ ($\kappa\epsilon/\gamma = 1$), we arrive at the following results:

$$\langle \hat{n} \rangle_{th} \to \sqrt{n_o} \frac{\Gamma(3/4)}{\Gamma(1/4)} \approx 0.338\sqrt{n_o}, \tag{39}$$

$$g_{th}^{(2)}(0) \to \frac{1}{4} \left[\frac{\Gamma(1/4)}{\Gamma(3/4)} \right]^2 \approx 2.188, \tag{40}$$

where we have used the fact that $\kappa\epsilon/\gamma = 1$ at threshold in Eq. (39). Thus the mean photon number at threshold is of the order of $\sqrt{n_o}$ and normalized photon number variance is $g_{th}^{(2)}(0) - 1 = 1.188$. The latter, being independent of scale factors, can be used to identify the threshold of oscillation.

Figure 2 shows the variation of mean photon number $\langle \hat{n} \rangle / \langle \hat{n} \rangle_{th}$ as a function of pump parameter a_1. The mean photon number grows monotonically as the pump parameter a_1 increases. The growth, which is slow below threshold, speeds up as threshold is approached becoming linear above threshold as a_1 increases. Note that the mean photon number at threshold is $\approx \sqrt{n_o}/3$ [see Eq. (39)]. Hence the parameter n_o can be interpreted as the square of mean photon number in the DPO at threshold. For comparison, the dashed curve shows the variation of photon number with pump parameter for a single-mode laser.

Figure 3(a) shows the variation of relative photon number fluctuations as a function of a_1. From Eq. (36), we see that

below threshold ($a_1<0$), the photon number variance $g^{(2)}(0)-1\equiv\langle:(\Delta\hat{n})^2:\rangle/\langle\hat{n}\rangle^2\rightarrow 2+1/2\bar{n}$ compared to $g^{(2)}(0)-1\rightarrow 1$ for thermal light or for a laser operating below threshold. Thus below threshold, the light from the DPO is more bunched than the light from a thermal source or from a laser operating below threshold. Even at threshold, the DPO with $g^{(2)}(0)-1=1.188$ is noisier than a laser with $g^{(2)}(0)-1=0.57$. Once above threshold, the photon number fluctuations in a DPO decrease rapidly as $g^{(2)}(0)-1\sim 1/a_1^2$. Figure 3(b) shows the variation of normalized third- and fourth-order moments of photon number fluctuations: $\alpha_3\equiv\langle:(\Delta\hat{n})^3:\rangle/\langle\Delta\hat{n}\rangle^3$ and $\alpha_4\equiv\langle:(\Delta\hat{n})^4:\rangle/\langle\hat{n}\rangle^4$. The quantity α_3 measures the skewness (lack of symmetry) of the distribution about the mean; a negative value of α_3 implies the distribution is skewed toward smaller (than the mean) values and a positive value implies skewness toward larger values. The quantity α_4 is a measure of kurtosis (the *peakedness*) of the distribution; large values of α_4 ($\alpha_4>3$) indicate a flatter distribution (compared to a Poisson distribution) and smaller values indicate a more peaked distribution. These moments rapidly decrease from their superthermal values below threshold to zero above threshold as the DPO crosses its threshold. As in the case of a laser, the changes described here take place over a pump parameter range given approximately by $|a_1|<10$. This corresponds to σ/n_o differing from its threshold value $\sigma/n_o=1$ by a very small amount $|\sigma/n_o-1|\leq 10/\sqrt{2n_o}$ [see Eq. (8)], which for $n_o=10^6$ amounts to $|\sigma/n_o-1|\leq 7\times 10^{-3}$. It is clear that although the overall behavior of the DPO in crossing the threshold is similar to that of a single-mode laser, there are important differences. Thus the DPO, in general, is noisier than a single-mode laser. Large relative photon number fluctuations of the DPO below and near threshold are due to the fact that in this regime of operation, the DPO cavity has no photons most of the time, but each time a pump photon is down converted to a pair of photons, the photon number in the DPO cavity surges for short periods (of the order of cavity lifetime) resulting in a small mean but large photon number fluctuations. This is also reflected in the form of the cavity photon number distribution p_n below threshold, which has a single peak at $n=0$ and a tail extending to large photon numbers. As the DPO crosses the threshold, the photon number distribution evolves into a distribution with a single peak at a nonzero value of n (corresponding to nonzero amplitude of oscillation) high above threshold. However, this transformation of the photon number distribution for the DPO follows a path different from that for a laser. To see this, we consider the photon number distribution itself.

C. Photon number distribution

The probability that the DPO cavity contains n photons is given by $p_n=\langle n|\hat{\rho}|n\rangle$. Using Eqs. (2) and (4), we can write

$$p_n=\int\int_{-\infty}^{\infty}dx_1dx_2\frac{(x_1x_2)^n}{n!}\exp(-x_1x_2)\mathcal{P}(x_1,x_2). \quad (41)$$

Substituting the distribution $\mathcal{P}(x_1,x_2)$ given in Eq. (4) and carrying out the integration, we obtain p_n,

$$p_{2n}=\frac{1}{N}\frac{(\sigma)^{2n}}{(2n)!}\sum_{m=0}^{\infty}\frac{(\sigma)^{2m}}{(2m)!}\left[\frac{\Gamma(m+n+1/2)}{\Gamma(m+n+n_o+1/2)}\right]^2, \quad (42)$$

$$p_{2n+1}=\frac{1}{N}\frac{(\sigma)^{2n+1}}{(2n+1)!}\sum_{m=0}^{\infty}\frac{(\sigma)^{2m+1}}{(2m+1)!}\left[\frac{\Gamma(m+n+3/2)}{\Gamma(m+n+n_o+3/2)}\right]^2, \quad (43)$$

where the normalization constant N is given by

$$N=\sum_{m=0}^{\infty}\frac{(2\sigma)^{2m}}{(2m)!}\left[\frac{\Gamma(m+1/2)}{\Gamma(m+n_o+1/2)}\right]^2. \quad (44)$$

Another expression for p_n, which is more suitable for near threshold operation, can be derived as follows. Near threshold, we can express x_1 and x_2 in terms of new variables u_1 and u_2 [Eqs. (6)] and write

$$p_n=\frac{4}{n!}\int_0^{\infty}du_1\int_0^{\infty}du_2\left[\frac{\sigma}{\sqrt{2n_o}}(u_1^2-u_2^2)\right]^n \times\exp\left[-\frac{\sigma}{\sqrt{2n_o}}(u_1^2-u_2^2)\right]\mathcal{P}(u_1,u_2). \quad (45)$$

Using the near threshold expression (7) for $\mathcal{P}(u_1,u_2)$, we find that p_n can be written as

$$p_n=\sum_{r=0}^{n}f_1(r)f_2(n-r), \quad (46)$$

where

$$f_1(r)=\frac{(a_1-a_2)^r}{r!\,2^{2r}}\frac{\Gamma(r+1/2)D_{[-(r+1/2)]}[(|a_2|-3a_1)/4]}{\Gamma(1/2)D_{(-1/2)}(-a_1)} \times\exp([(a_1+|a_2|)(|a_2|-7a_1)/64]), \quad (47)$$

$$f_2(r)=\frac{(-1)^r(2r-1)!!}{2^r(r)!}\sqrt{\frac{4|a_2|}{3|a_2|-a_1}}\left[\frac{a_1+|a_2|}{3|a_2|-a_1}\right]^r. \quad (48)$$

Figure 4 shows p_n as a function of n below, at, slightly above, and much above threshold. Below, threshold p_n has a sharp peak at $n=0$ and a long tail reflecting large photon number fluctuations. In passing the threshold $a_1=0$, photon number distribution p_n develops into a bimodal distribution; in addition to the peak at $n=0$, a broad maximum centered at a nonzero value of n begins to emerge. With further increase in the pump parameter, the peak at $n=0$ is suppressed rapidly while the broad maximum sharpens into a Gaussian centered at increasingly larger values of photon number n. In addition, p_n displays a peculiar steplike behavior [see Fig. 5], which is particularly prominent for small values of n throughout the region of threshold. In contrast to this, the photon number distribution for the single-mode laser oscillator has a single peak throughout the threshold region and in passing the threshold the peak at $n=0$ below threshold evolves smoothly into a peak at a nonzero value of n above threshold [16,17]. The DPO does ultimately reach a state where the relative photon number fluctuations go to zero as is the case for a

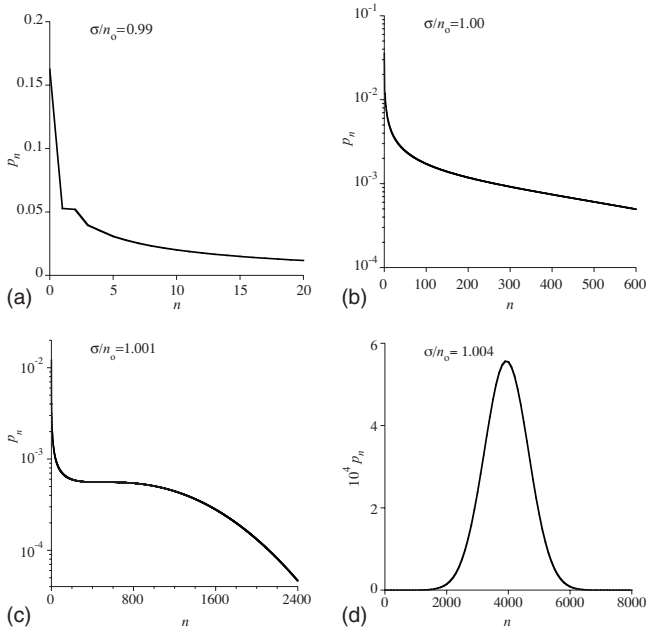

FIG. 4. DPO photon number distribution p_n for $n_0=10^6$ and several different operating points near threshold: (a) $\sigma/n_o=0.99$, (b) $\sigma/n_o=1.00$, (c) $\sigma/n_o=1.001$, and (d) $\sigma/n_o=1.004$. The distributions, although plotted as continuous curves, are meaningful only for integer values of n.

single-mode laser above threshold. However, the phase properties of the light from the DPO continue to carry the signatures of its quantum nature which manifests itself in field quadrature squeezing. In this sense, the state of the DPO continues to be distinct from that of a laser oscillator even high above threshold.

We can also calculate the photon counting distribution $p(m,T)$, the probability of detecting m photons in time T by a detector placed outside the cavity. We note that the operator for the photon flux leaving the DPO cavity, in the positive-P representation, is $\hat{I}\equiv 2\gamma\hat{n}\rightarrow 2\gamma x_1 x_2$, where 2γ is the photon number decay rate from the cavity and $\hat{n}$ is the photon number operator. For short counting interval T such that $2\gamma T \ll 1$, the time integrated flux for a detector of quantum efficiency α can be approximated as $\alpha\int_t^{t+T} dt 2\gamma x_1 x_2 \approx \alpha 2\gamma T x_1 x_2$. Then the photon counting distribution $p(m,T)$ can be written as

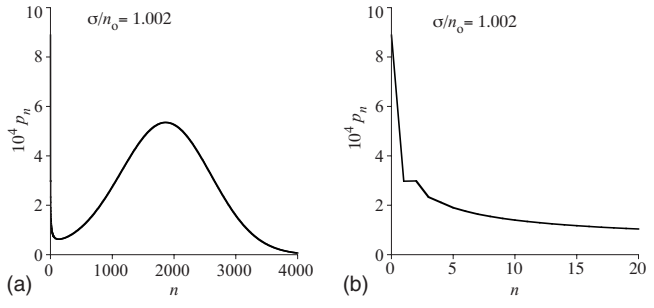

FIG. 5. Steplike behavior of photon number distribution p_n for the DPO near threshold for $n_0=10^6$ and $\sigma/n_o=1.002$. (b) shows the peak near $n=0$ in detail. The distributions are meaningful for only integer values of n.

$$P(m,T)=\frac{4}{m!}\int_0^\infty du_1\int_0^\infty du_2\left[\frac{\beta\sigma}{\sqrt{2n_o}}(u_1^2-u_2^2)\right]^n \times\exp\left[-\frac{\beta\sigma}{\sqrt{2n_o}}(u_1^2-u_2^2)\right]\mathcal{P}(u_1,u_2), \tag{49}$$

where $\beta=\alpha 2\gamma T$. A comparison of this equation to Eq. (44) shows that it can be obtained form Eq. (44) with the replacement $\sigma\rightarrow\beta\sigma$. We can then derive expressions such as Eqs. (45)–(47) for $P(m,T)$. The behavior of $P(m,T)$ for arbitrary time interval T below threshold was discussed in great detail in Ref. [13] and will not be pursued further here.

III. NONDEGENERATE PARAMETRIC OSCILLATOR

In a nondegenerate parametric oscillator, a nonlinear crystal placed inside an optical cavity down converts a photon in pump mode $\hat{a}_3$ into one photon each in two nondegenerate modes $\hat{a}_1$ and $\hat{a}_2$ also referred to as signal and idler modes. Hamiltonian for this system can be written as

$$\hat{H}=i\hbar\kappa(\hat{a}_1^\dagger\hat{a}_2^\dagger\hat{a}_3-\hat{a}_1\hat{a}_2\hat{a}_3^\dagger)+i\hbar\gamma_3\varepsilon(\hat{a}_3^\dagger-\hat{a}_3)+\hat{H}_{loss}, \tag{50}$$

where κ is the mode-coupling constant which can be expressed in terms of nonlinear crystal parameters and $\hat{H}_{loss}$ describes mode losses. Mode $\hat{a}_3$ is excited by a classical pump field of frequency ω_3 and dimensionless amplitude ε, such that $|\varepsilon|^2$ gives the number of pump photons incident on the cavity in one lifetime of the cavity $(2\gamma_3)^{-1}$. If the cavity lifetime $((2\gamma_3)^{-1})$ at pump frequency is short compared to the cavity lifetime $((2\gamma)^{-1})$ at down-converted frequencies so that $(\gamma_3\gg\gamma)$, a typical situation, we can eliminate the pump mode $\hat{a}_3$ adiabatically. Then, if $\hat{\rho}$ represents the density matrix for the subharmonic fields, we can introduce the corresponding phase-space density $\mathcal{P}$ in the positive-P representation by [22]

$$\hat{\rho}=\int\int_{\mathcal{D}} d^2\alpha_1 d^2\alpha_{1*} d^2\alpha_2 d^2\alpha_{2*}\frac{|\alpha_1\rangle|\alpha_2\rangle\langle\alpha_{1*}|\langle\alpha_{2*}|}{\langle\alpha_{1*}|\alpha_1\rangle\langle\alpha_{2*}|\alpha_2\rangle}\mathcal{P}(\vec{\alpha}), \tag{51}$$

where $\mathcal{D}$ is a suitably chosen domain in the eight-dimensional phase space spanned by the complex variables α_1, α_2, α_{1*}, and α_{2*} and $\mathcal{P}(\vec{\alpha})\equiv\mathcal{P}(\alpha_1,\alpha_2,\alpha_{1*},\alpha_{2*})$ is real, positive, and normalized to unity. Complex variables α_i and α_{i*} are associated with the operators $\hat{a}_i$ and $\hat{a}_i^\dagger$ by $\hat{a}_i|\alpha_i\rangle=\alpha_i|\alpha_i\rangle$ and $\langle\alpha_{i*}|\hat{a}_i^\dagger=\alpha_{i*}\langle\alpha_{i*}|$. As already noted in the discussion of the DPO, in the positive-P representation, α_i and α_{i*} are not complex conjugates of each other. Using the density matrix in Eq. (51) in terms of positive-P function, the equation of motion for the density matrix leads to the following Fokker-Planck equation [18,23,24]

$$\frac{\partial \mathcal{P}(\vec{\alpha})}{\partial \tau} = -\frac{\partial}{\partial \alpha_1}\left[-\alpha_1 + \frac{\sigma}{n_o}\alpha_{2*} - \frac{2}{n_o}\alpha_{2*}\alpha_1\alpha_2\right]\mathcal{P}(\vec{\alpha}) + \frac{1}{n_o}\frac{\partial^2}{\partial\alpha_1\,\partial\,\alpha_2}(\sigma - 2\alpha_1\alpha_2)\mathcal{P}(\vec{\alpha}) - \frac{\partial}{\partial \alpha_2}\left[-\alpha_2 + \frac{\sigma}{n_o}\alpha_{1*} - \frac{2}{n_o}\alpha_{1*}\alpha_1\alpha_2\right]\mathcal{P}(\vec{\alpha}) - \frac{\partial}{\partial \alpha_{1*}}\left[-\alpha_{1*} + \frac{\sigma}{n_o}\alpha_2 - \frac{2}{n_o}\alpha_{1*}\alpha_{2*}\alpha_2\right]\mathcal{P}(\vec{\alpha}) + \frac{1}{n_o}\frac{\partial^2}{\partial\alpha_{1*}\,\partial\,\alpha_{2*}}(\sigma - 2\alpha_{1*}\alpha_{2*})\mathcal{P}(\vec{\alpha}) - \frac{\partial}{\partial \alpha_{2*}}\left[-\alpha_{2*} + \frac{\sigma}{n_o}\alpha_1 - \frac{2}{n_o}\alpha_{1*}\alpha_{2*}\alpha_1\right]\mathcal{P}(\vec{\alpha}). \tag{52}$$

Here, τ is time measured in units of γ^{-1}, $\sigma = 2\gamma_3\varepsilon/\kappa$ is a dimensionless measure of pump field amplitude, and parameter $n_o = 2\gamma\gamma_3/\kappa^2$ is proportional to the square of the number of photons in the NDPO at threshold. The threshold condition is given, as before, by $\sigma/n_o \equiv \kappa\epsilon/\gamma = 1$.

These equations describe evolution of $\mathcal{P}(\vec{\alpha})$ in an eight-dimensional phase space. However, a close inspection of this equation shows that a trajectory starting initially in the four-dimensional subspace $\alpha_2 = \alpha_{1*}$, $\alpha_{2*} = (\alpha_{1*})^*$ remains confined to this subspace [23,25]. Since the initial state, the vacuum state, lies in this four-dimensional subspace, we can restrict our discussion to this subspace. This conclusion also follows from the observation that in terms of operators $\hat{b}_1 = (\hat{a}_1 + \hat{a}_2)/\sqrt{2}$ and $\hat{b}_2 = -i(\hat{a}_1 - \hat{a}_2)/\sqrt{2}$, the Hamiltonian of Eq. (50) can be transformed into a Hamiltonian for two independent degenerate parametric oscillators with annihilation operators $\hat{b}_1$ and $\hat{b}_2$,

$$\hat{H} = \frac{i}{2}\hbar\kappa[(\hat{b}_1^{\dagger 2}\hat{a}_3 - \hat{b}_1^2\hat{a}_3^\dagger) + (\hat{b}_2^{\dagger 2}\hat{a}_3 - \hat{b}_2^2\hat{a}_3^\dagger)] + i\hbar\gamma_3\varepsilon(\hat{a}_3^\dagger - \hat{a}_3) + \hat{H}_{loss}. \tag{53}$$

Then by introducing the real variables

$$x_1 = (\alpha_1 + \alpha_2)/\sqrt{2}, \quad x_2 = -i(\alpha_1 - \alpha_2)/\sqrt{2}, \tag{54}$$

$$x_3 = (\alpha_{1*} + \alpha_{2*})/\sqrt{2}, \quad x_4 = i(\alpha_{1*} - \alpha_{2*})/\sqrt{2}, \tag{55}$$

the Fokker-Planck equation for the probability distribution $p \equiv p(\vec{x})$ with $\vec{x} \equiv (x_1, x_2, x_3, x_4)$ can be written as

$$\frac{\partial p}{\partial t} = -\frac{\partial}{\partial x_1}\left[-x_1 + \frac{x_3}{n_o}\{\sigma - (x_1^2 + x_2^2)\}\right]p + \frac{1}{2n_o}\frac{\partial^2}{\partial x_1^2}[\{\sigma - (x_1^2 + x_2^2)\}p] - \frac{\partial}{\partial x_2}\left[-x_2 + \frac{x_4}{n_o}\{\sigma - (x_1^2 + x_2^2)\}\right]p + \frac{1}{2n_o}\frac{\partial^2}{\partial x_2^2}[\{\sigma - (x_1^2 + x_2^2)\}p] - \frac{\partial}{\partial x_3}\left[-x_3 + \frac{x_1}{n_o}\{\sigma - (x_3^2 + x_4^2)\}\right]p + \frac{1}{2n_o}\frac{\partial^2}{\partial x_3^2}[\{\sigma - (x_3^2 + x_4^2)\}p] - \frac{\partial}{\partial x_4}\left[-x_4 + \frac{x_2}{n_o}\{\sigma - (x_3^2 + x_4^2)\}\right]p + \frac{1}{2n_o}\frac{\partial^2}{\partial x_4^2}[\{\sigma - (x_3^2 + x_4^2)\}p]. \tag{56}$$

The steady-state solution of this Fokker-Planck equation is found to be [18]

$$p(\vec{x}) = \text{const}[\{\sigma - (x_1^2 + x_2^2)\}\{\sigma - (x_3^2 + x_4^2)\}]^{n_o - 1} \times \exp[2x_1x_3 + 2x_2x_4], \tag{57}$$

where $(x_1^2 + x_2^2)$, $(x_3^2 + x_4^2) < \sigma$. Once again using the fact that the parameter $n_o \approx 10^6 - 10^8$ is very large, we can introduce scaled pseudoquadrature variables

$$u_1 = \left(\frac{n_o}{8\sigma^2}\right)^{1/4}(x_1 + x_3), \quad u_2 = \left(\frac{n_o}{8\sigma^2}\right)^{1/4}(x_1 - x_3), \tag{58}$$

$$u_3 = \left(\frac{n_o}{8\sigma^2}\right)^{1/4}(x_2 + x_4), \quad u_4 = \left(\frac{n_o}{8\sigma^2}\right)^{1/4}(x_2 - x_4) \tag{59}$$

and write the steady-state distribution to an excellent approximation as

$$P(\vec{u}) \approx \frac{1}{\mathcal{N}}\exp[a_1(u_1^2 + u_3^2) + a_2(u_2^2 + u_4^2) - 1/2\{(u_1^2 + u_2^2 + u_3^2 + u_4^2)^2 + 4(u_1^2 + u_3^2)(u_2^2 + u_4^2)\}], \tag{60}$$

where the pump parameters a_1 and a_2 are given by

$$a_1 = \sqrt{2n_o}(\sigma/n_o - 1) = \sqrt{2n_o}(\kappa\varepsilon/\gamma - 1), \tag{61}$$

$$a_2 = -\sqrt{2n_o}(\sigma/n_o + 1) = -\sqrt{2n_o}(\kappa\varepsilon/\gamma + 1). \tag{62}$$

The normalization constant $\mathcal{N}$, determined by the condition $\int P(\vec{u})d\vec{u} = 1$, is given by

$$\mathcal{N} = \pi^2\sqrt{\frac{\pi}{2}}\exp(a_1^2/2)\int_0^\infty ds\,\exp\left[-\frac{1}{2}(s - a_1)^2 + \frac{1}{2}(3s + |a_2|)^2\right]\text{erfc}\left(\frac{3s + |a_2|}{\sqrt{2}}\right), \tag{63}$$

where erfc(z) is the complement of error function given by

$$\text{erfc}(z) = \frac{2}{\sqrt{\pi}}\int_z^\infty dt e^{-t^2} = 1 - \text{erf}(z). \tag{64}$$

for large values of its argument, this function has the asymptotic forms

$$\mathrm{erfc}(z) = \begin{cases} \dfrac{\exp(-z^2)}{\sqrt{\pi}z}\left[1 - \dfrac{1}{2z^2} + \dfrac{3}{4z^4} - \cdots\right], & z \to \infty \\ 2 - \dfrac{\exp(-z^2)}{\sqrt{\pi}|z|}\left[1 - \dfrac{1}{2z^2} + \dfrac{3}{4z^4} - \cdots\right], & z \to -\infty. \end{cases} \tag{65}$$

The form of the distribution function $P(\vec{u})$ in Eq. (60) is similar to the joint probability distribution for two-mode lasers [16,17] if we identify pseudoquadrature variables with real field amplitudes in two-mode lasers. It describes oscillators u_1 and u_3 with pump parameter a_1 and oscillators u_2 and u_4 with pump parameter a_2. The variables u_1 and u_3 represents unsqueezed quadratures and variables u_2 and u_4 correspond to squeezed quadratures.

Pump parameter a_2 is always a large negative number, its magnitude always being larger than $\sqrt{2n_o} \gg 1$. This means that u_2 and u_4 always remain below threshold and their distributions are centered at zero and have narrow width ($\approx 1/|a_2|$). Pump parameter a_1 determines the operating point for the oscillators u_1 and u_3 and therefore the operating point of the NDPO. The threshold of oscillation for the NDPO is $a_1=0$ or $\kappa\epsilon/\gamma=1$. Pump parameter a_1 is negative below and positive above threshold. Depending on the pump parameter a_1, we can further simplify the distribution function.

Below threshold $\sigma/n_o=\kappa\varepsilon/\gamma<1$ where both a_1 and a_2 are large negative quantities, we can approximate the positive-P distribution by

$$P(\vec{u}) \approx \frac{|a_1||a_2|}{\pi^2}\exp[-|a_1|(u_1^2+u_3^2) - |a_2|(u_2^2+u_4^2)]. \tag{66}$$

Thus below threshold, the P distribution can be expressed as the product of four independent Gaussian distributions with zero mean. Moments of u_i $(i=1,2,3,4)$ can be expressed in terms of their variances as

$$\langle u_i^{2n+1}\rangle = 0,$$

$$\langle u_i^{2n}\rangle = (2n-1)!!\left(\frac{1}{2|a_i|}\right)^n, \tag{67}$$

where n is an integer and $a_3=a_1$ and $a_4=a_2$. Complete photon statistics, including photoelectron counting distribution, intensity correlations, and waiting time distribution, in this limit, have been discussed already [25].

Near threshold $a_1 \approx 0 (\kappa\varepsilon \approx \gamma)$, parameter $a_2 \approx -\sqrt{8n_o}$ is still a large negative number. This means u_2 and u_4 continue to behave as independent Gaussian random variables with zero mean and their distributions are dominated by their small values. On the other hand, as a_1 changes from below to above threshold, u_1 and u_3 are no longer Gaussian. In this range, the steady-state distribution $P(\vec{u})$ given in Eq. (60) can be approximated by

$$\tilde{P}(\vec{u}) \approx \left(\frac{|a_2|}{\pi}\right)\exp[-|a_2|(u_2^2+u_4^2)] \times\left(\frac{1}{Q}\exp\left[a_1(u_1^2+u_3^2) - \tfrac{1}{2}(u_1^2+u_3^2)^2\right]\right), \tag{68}$$

where the normalization constant Q is given by

$$Q = \int\int_{-\infty}^{\infty} du_1 du_3 \exp\left[a_1(u_1^2+u_3^2) - \tfrac{1}{2}(u_1^2+u_3^2)^2\right] = \pi^{3/2}\exp\left(\tfrac{1}{2}a_1^2\right)\mathrm{erfc}(-a_1/\sqrt{2}). \tag{69}$$

The distribution in Eq. (68) indicates that u_2 and u_4 behave as statistically independent Gaussian random variables whereas u_1 and u_3 are non-Gaussian, strongly coupled, and statistically correlated random variables. Since the distribution depends only on u_1^2 and u_3^2, it is an even function of u_1 and u_3. Hence the odd-order moments of u_1 and u_3 vanish: $\langle u_1^{2n+1}\rangle = 0 = \langle u_3^{2n+1}\rangle$. Furthermore, since u_1 and u_3 occur on equal footing in the distribution, their nonzero moments are equal: $\langle u_1^{2n}\rangle = \langle u_3^{2n}\rangle$. Normalization constant Q treated as a function of a_1 also serves as a moment generating function as in the case of two-mode lasers [16,17]. Thus moments of u_1^2 and u_3^2 can be calculated from

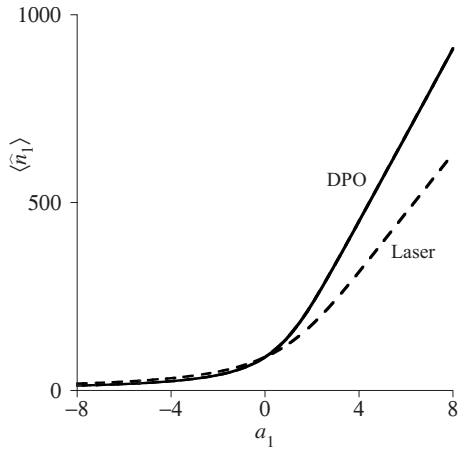

FIG. 6. Mean photon number in either mode of the NDPO as a function of pump parameter a_1 for $n_o=10^5$. For comparison, the (dashed) curve for the laser is also shown.

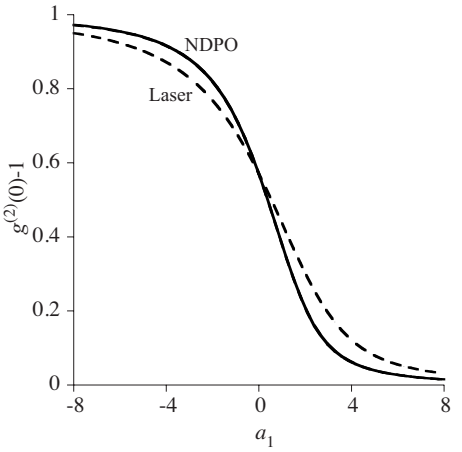

FIG. 7. Normalized photon number variance for either mode of an NDPO as a function of pump parameter a_1. The dashed curve is for the laser.

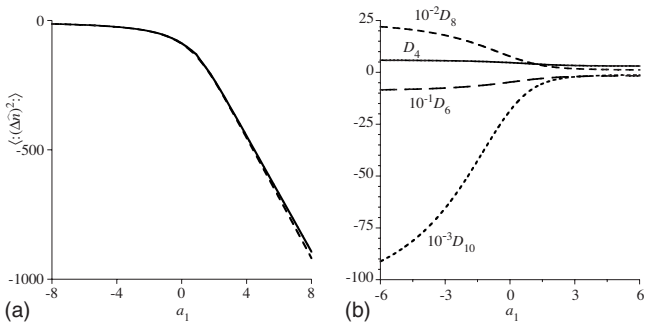

FIG. 8. (a) Variation of normally ordered variance of photon number difference variable. Solid curve is computed from Eq. (60) and the dashed curve from Eq. (68). (b) Normalized higher-order moments D_{2r} for different values of r. Negative value of moments indicates nonclassical behavior.

$$\langle (u_1^2+u_3^2)^n\rangle = \int\int_{-\infty}^{\infty} du_1 du_3 (u_1^2+u_3^2)^n \times \exp\left[a(u_1^2+u_3^2)-\tfrac{1}{2}(u_1^2+u_3^2)^2\right] = \frac{\partial^n \ln Q}{\partial a_1^n}, \tag{70}$$

$$\langle u_1^{2n}\rangle = \langle u_3^{2n}\rangle. \tag{71}$$

As an example, using Eqs. (69)–(71) we obtain, for $n=1$,

$$\langle u_1^2\rangle = \langle u_3^2\rangle = \frac{1}{2}\left[a_1 + \sqrt{\frac{2}{\pi}}\frac{\exp(-a_1^2/2)}{\operatorname{erfc}(-a_1/\sqrt{2})}\right]. \tag{72}$$

A. Photon number fluctuations

The steady-state distribution $\tilde{P}(\vec{u})$ given in Eq. (68) has a simple form and allows us to derive analytical expressions for the photon statistics and compare them to the results obtained from the distribution $P(\vec{u})$ given in Eq. (60). We find that the results obtained from both Eqs. (68) and (60) are in excellent agreement with the results obtained from the exact distribution $p(\vec{x})$ given in Eq. (57) for n_o larger than 10^4.

The mean photon number $\langle \hat{n}_i\rangle = \langle \alpha_{i*}\alpha_i\rangle$ for the ith mode, calculated by using the distribution (68), is given by

$$\langle \hat{n}_1\rangle = \sqrt{\frac{\sigma^2}{2n_o}}(\langle u_1^2\rangle - \langle u_2^2\rangle) = \sqrt{\frac{\sigma^2}{8n_o}}\left[a_1 + \sqrt{\frac{2}{\pi}}\frac{\exp(-a_1^2/2)}{\operatorname{erfc}(-a_1/\sqrt{2})} - \frac{1}{|a_2|}\right] \tag{73}$$

and normally ordered variance of $\hat{n}_1$ is given by

$$\langle :(\Delta\hat{n}_1)^2:\rangle = \langle (\alpha_{1*}\alpha_1)^2\rangle - \langle \alpha_{1*}\alpha_1\rangle^2 = \frac{\sigma^2}{8n_o}[\langle (u_1^2+u_3^2)^2\rangle + \langle (u_2^2+u_4^2)^2\rangle - 4\langle u_1^2+u_3^2\rangle\langle u_2^2+u_4^2\rangle - 4\langle u_1^2-u_2^2\rangle^2] = \frac{\sigma^2}{8n_o}\left[1+\frac{1}{|a_2|^2} - \left(a_1 + \sqrt{\frac{2}{\pi}}\frac{\exp(-a_1^2/2)}{\operatorname{erfc}(-a_1/\sqrt{2})}\right)\right.$$

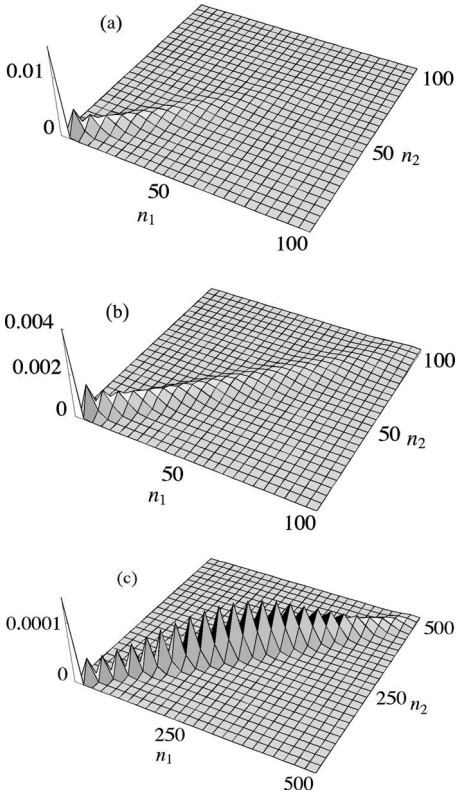

FIG. 9. Joint photon number distribution $p(n_1,n_2)$ for the NDPO (a) below, (b) at, and (c) above threshold for $n_o=10^5$.

$$\left.\times\frac{2}{|a_2|} + \sqrt{\frac{2}{\pi}}\frac{\exp(-a_1^2/2)}{\operatorname{erfc}(-a_1/\sqrt{2})}\right)\Bigg]. \tag{74}$$

For comparison, the mean and normally ordered variance calculated by using the distribution of Eq. (60) is [18]

$$\langle \hat{n}_1\rangle = \sqrt{\frac{\sigma^2}{8n_o}}\left[a_1 - a_2 + \frac{1}{\mathcal{N}}\sqrt{\frac{\pi}{2}}[\exp(a_1^2/2)\operatorname{erfc}(-a_1/\sqrt{2}) - \exp(a_2^2/2)\operatorname{erfc}(-a_2/\sqrt{2})]\right], \tag{75}$$

$$\langle :(\Delta\hat{n}_1)^2:\rangle = \frac{\sigma^2}{4n_o}\left[\frac{\partial\langle u_1^2\rangle}{\partial a_1} + \frac{\partial\langle u_2^2\rangle}{\partial a_2} - 4\frac{\partial\langle u_2^2\rangle}{\partial a_1} - 4\langle u_1^2\rangle\langle u_2^2\rangle\right],$$

$$= \frac{\sigma^2}{64n_o}\left[-14 + (10a_2 - 14a_1)\langle u_1^2\rangle + (10a_1 - 14a_2)\langle u_2^2\rangle - 32(\langle u_1^2\rangle - \langle u_2^2\rangle)^2 + \frac{5}{\mathcal{N}}\left\{2 + \sqrt{\frac{\pi}{2}}a_1 \times \exp(a_1^2/2)\operatorname{erfc}(-a_1/\sqrt{2}) + \sqrt{\frac{\pi}{2}}a_2 \times \exp(a_2^2/2)\operatorname{erfc}(-a_2/\sqrt{2})\right\}\right], \tag{76}$$

where the normalization constant $\mathcal{N}$ is given by Eq. (63) and

$$\langle u_1^2\rangle = \frac{1}{16}\left[-(a_1-3a_2)+\frac{1}{\mathcal{N}}\sqrt{\frac{\pi}{2}}\left\{3\exp(a_1^2/2)\,\mathrm{erfc}\left(-\frac{a_1}{\sqrt{2}}\right)-\exp(a_2^2/2)\,\mathrm{erfc}\left(-\frac{a_2}{\sqrt{2}}\right)\right\}\right], \tag{77}$$

$$\langle u_2^2\rangle = \frac{1}{16}\left[-(a_2-3a_1)+\frac{1}{\mathcal{N}}\sqrt{\frac{\pi}{2}}\left\{3\exp(a_2^2/2)\,\mathrm{erfc}\left(-\frac{a_2}{\sqrt{2}}\right)-\exp(a_1^2/2)\,\mathrm{erfc}\left(-\frac{a_1}{\sqrt{2}}\right)\right\}\right]. \tag{78}$$

Equations (75) and (76) reduce, respectively, to Eqs. (73) and (74) when we use the fact that a_2 is a large negative number.

Figure 6 shows the mean photon number calculated from Eqs. (73) and (75) as a function of pump parameter a_1 for $n_o=10^5$. We find that even for this somewhat smaller value of n_o, the two curves are indistinguishable. The agreement is expected to be even better for larger values of n_o. Below threshold ($a_1<0$), the mean photon number is small, as expected, and increases slowly as a_1 approaches the threshold. As a_1 passes the threshold, the mean increases rapidly and grows linearly with pump parameter above threshold. This behavior is similar to that for a single-mode laser [16]. Far below threshold ($a_1<0$) and far above threshold ($a_1>0$), the expression for the mean leads to

$$\langle \hat{n}_1\rangle \to \begin{cases} \sqrt{\dfrac{\sigma^2}{8n_o}}\left[\dfrac{1}{|a_1|}-\dfrac{1}{|a_2|}\right], & \text{below threshold } (|a_2|\gg|a_1|>5) \\ \sqrt{\dfrac{\sigma^2}{8n_o}}\left[a_1+\dfrac{1}{\sqrt{2\pi}}\exp(-a_1^2/2)-\dfrac{1}{|a_2|}\right], & \text{above threshold } (|a_2|\gg a_1>5). \end{cases} \tag{79}$$

Figure 7 shows the behavior of normalized variance $g^{(2)}(0)-1\equiv\langle:(\Delta\hat{n}_1)^2:\rangle/\langle\hat{n}_1\rangle^2$ near threshold as a function of mean photon number $\langle\hat{n}_1\rangle$ for $n_o=10^5$. Once again, the results obtained from the two distributions (60) and (68) are indistinguishable in Fig. 7. For comparison, $g^{(2)}(0)-1$ for a single-mode laser [16] is also shown (dashed curve) in the same figure. For this comparison, we chose the saturation photon number for the laser, which is analogous n_o, to be such that the laser has the same mean photon number at threshold as either of the NDPO modes. We see that below threshold $g^{(2)}(0)-1$ for the NDPO is nearly unity indicating that below threshold, fluctuations of light in each mode of the NDPO are thermal. Much above threshold, $g^{(2)}(0)-1$ for the NDPO decreases rapidly to zero indicating an approach to a state with a relatively well-defined photon number. These observations are in agreement with the expressions for normalized variance obtained from Eqs. (73) and (74) below threshold ($a_1<0$) and above threshold ($a_1>0$),

$$g^{(2)}(0)-1 \to \begin{cases} 1-\dfrac{8}{|a_1|}\left(\dfrac{1}{|a_1|}+\dfrac{2}{|a_2|}\right), & \text{below threshold:}(|a_2|\gg|a_1|\gg 1) \\ \dfrac{1}{a_1^2}-\dfrac{1}{a_1|a_2|}, & \text{above threshold:}(|a_2|\gg a_1\gg 1). \end{cases} \tag{80}$$

It is interesting to note that the curve for the NDPO follows the curve for a laser. This is in contrast to the behavior of the DPO, which has superthermal fluctuations below threshold and differs significantly from the curve for the laser even in the threshold region.

From the discussion in the preceding two paragraphs, we see that the threshold behavior of both modes of the NDPO is similar to that of a laser; the quantum character of NDPO light is not reflected in photon number variances of the modes. However, the nonclassical nature of the light from the NDPO is reflected in the variance and higher-order moments of photon number difference (PND) variable $\hat{n}_1-\hat{n}_2=\Delta\hat{n}$. Using the distribution given by Eq. (68), we find that the normally ordered variance of the photon number difference is given by

$$\langle:(\Delta\hat{n})^2:\rangle \approx -n_o\left(\frac{\sigma}{n_o}\right)^2\frac{1}{|a_2|}\left[a_1+\sqrt{\frac{2}{\pi}}\frac{\exp(-a_1^2/2)}{\mathrm{erfc}(-a_1/\sqrt{2})}\right]. \tag{81}$$

If we use the distribution (60), we can express normally ordered variance of the photon number difference $\Delta\hat{n}$ as

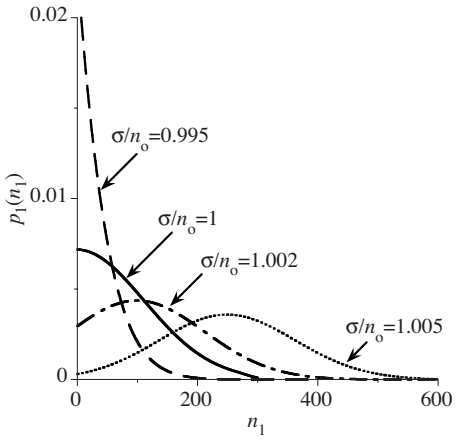

FIG. 10. Photon number distribution for either mode of the DPO below ($\sigma/n_o=0.995$), at ($\sigma/n_o=1.00$), and above threshold ($\sigma/n_o=1.002$ and 1.005).

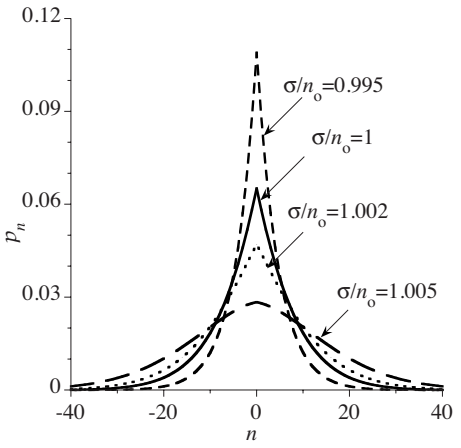

FIG. 11. Distribution of photon number difference variable $n \equiv n_1 - n_2$, below ($\sigma/n_o<1$), at ($\sigma/n_o=1$), and above threshold ($\sigma/n_o>1$) for $n_o=10^5$.

$$\langle :(\Delta\hat{n})^2: \rangle = -\frac{\sigma^2}{n_o}\left[4\langle u_1^2\rangle\langle u_2^2\rangle + 2\frac{\partial\langle u_2^2\rangle}{\partial a_1}\right]$$

$$= -\frac{\sigma^2}{8n_o}\left[3 + 2(3a_1 - a_2)\langle u_1^2\rangle - \frac{1}{\mathcal{N}}\left\{1 + \sqrt{\frac{\pi}{2}}a_1 \exp(a_1^2/2) \times \mathrm{erfc}(-a_1/\sqrt{2})\right\}\right]. \quad (82)$$

Once again, on utilizing the fact $|a_2| \gg 1$, we find that Eq. (82) reduces to Eq. (81).

The most significant aspect of Eqs. (81) and (82) is that the normally ordered variance of the photon number difference variable is a negative quantity reflecting nonclassical behavior of the light from the NDPO [18,37]. This nonclassical feature of the variance of difference variable survives even in the semiclassical limit $\sigma/n_o \gg 1$, which corresponds to the NDPO operating high above threshold.

Figure 8(a) shows a comparison of the variance $\langle :(\Delta\hat{n})^2: \rangle$ computed from Eq. (60) (solid curve) and Eq. (68) (dashed curve) as a function of pump parameter a_1 near threshold for $n_o=10^5$. For these figures, a_1 ranges approximately from -8 to 8 corresponding to $|\sigma/n_o - 1| < 2\%$. Below threshold, the variance of the difference variable is small and negative and the two curves coincide. As the pump parameter increases and the NDPO crosses threshold, the difference between the two curves begins to show up. This is because with increasing a_1, the peak of the steady-state distribution begins to explore larger values of u_1 and u_3 so that the contribution of the terms that were dropped from Eq. (60) to arrive at Eq. (68) begins to show up. These terms are particularly significant for the moments of photon number difference variable. We also find that these results are in agreement with the $\langle :(\Delta\hat{n})^2: \rangle$ obtained by using the exact distribution given in Eq. (57). It is interesting to note that near threshold, the curve for normally ordered variance follows the mean $\langle \hat{n}_1 \rangle$ plotted in Fig. 6 except that it has opposite sign, which suggests that $\langle :(\Delta\hat{n})^2: \rangle \approx -\langle \hat{n}_1 \rangle$ near threshold.

Higher-order moments of $\Delta\hat{n} \equiv \hat{n}_1 - \hat{n}_2$ can be calculated by using a method similar to that for two-mode lasers [17,34,35] or using Eq. (91). We find that even-order moments $\langle :(\Delta\hat{n})^{2r}: \rangle$ are positive quantities for $r=2,4,6,\ldots$ and negative quantities for $r=1,3,5,\ldots$. Negative values of $\langle :(\Delta\hat{n})^{2r}: \rangle$ violate classical inequalities reflecting the quantum nature of the NDPO light. These violations can be traced to strong intermode photon number correlations relative to photon autocorrelations for the two modes. Relative size of these violations can be characterized by introducing normalized moments of $\Delta\hat{n}$,

$$D_{2r} \equiv \frac{\langle :(\Delta\hat{n})^{2r}: \rangle}{|\langle :(\Delta\hat{n})^2: \rangle|^r}, \quad r = 1,2,3,\ldots. \quad (83)$$

Figure 8(b) shows the variation of normalized moments for $2r=4,6,8,10$ as functions of pump parameter a_1 near threshold. Above threshold, these moments approach the values ± 1. Recall that odd-order moments of $\hat{n}$ vanish.

It is clear from this discussion that even though the two modes of the NDPO behave individually like a single-mode laser, the quantum nature of the NDPO light survives in variance and higher-order moments of photon number difference variable even high above threshold. Similar comments hold for squeezing, which is not present in either of the two modes but the combination modes $\hat{b}_1 = (\hat{a}_1 + \hat{a}_2)/\sqrt{2}$ and $\hat{b}_1 = -i(\hat{a}_1 - \hat{a}_2)/\sqrt{2}$ retain it even in the semiclassical limit [18].

B. Joint photon number distribution

In view of the nonclassical character of the variable $\hat{n}=\hat{n}_1-\hat{n}_2$, another quantity of interest is the joint photon number distribution $p(n_1,n_2)$ for the probability of n_1 photons in mode $\hat{a}_1$ and n_2 photons in mode a_2. This distribution is given by

$$p(n_1,n_2) \equiv \left\langle :\frac{(\hat{a}_1^\dagger \hat{a}_1)^{n_1}}{n_1!}\frac{(\hat{a}_2^\dagger \hat{a}_2)^{n_2}}{n_2!}\exp[-(\hat{a}_1^\dagger \hat{a}_1+\hat{a}_2^\dagger \hat{a}_2)]: \right\rangle \rightarrow \left\langle \frac{(\alpha_{1*}\alpha_1)^{n_1}}{n_1!}\frac{(\alpha_{2*}\alpha_2)^{n_2}}{n_2!}\exp[-(\alpha_{1*}\alpha_1+\alpha_{2*}\alpha_2)] \right\rangle_P, \tag{84}$$

where the last averaging is with respect to the positive-P function. Using the distribution function given in Eq. (57), we obtain $p(n_1,n_2)$ for $n_1>n_2$ as

$$p(n_1,n_2)=\frac{1}{Z}\frac{1}{n_1!\,n_2!}\sum_{m=0}^{\infty}\frac{(\sigma/2)^{2m+n_1+n_2+|n_1-n_2|}}{m!\,(m+|n_1-n_2|)!}\left[\frac{\Gamma\left(m+\frac{1}{2}(n_1+n_2)+\frac{1}{2}|n_1-n_2|+1\right)\Gamma(n_o)}{\Gamma\left(n_o+m+\frac{1}{2}(n_1+n_2)+\frac{1}{2}|n_1-n_2|+1\right)}\right]^2, \tag{85}$$

where the normalization constant Z is given by

$$Z=\sum_{m=0}^{\infty}\frac{(\sigma)^{2m}}{(m!)^2}\left[\frac{\Gamma(m+1)\Gamma(n_o)}{\Gamma(n_o+m+1)}\right]^2. \tag{86}$$

$p(n_1,n_2)$ for $n_1<n_2$ is obtained by interchanging n_1 and n_2. Figure 9 shows the form of the joint photon number distribution below, at, and above threshold.

Photon number distribution for mode 1 can be obtained by summing $p(n_1,n_2)$ over n_2,

$$p_1(n_1)=\sum_{n_2=0}^{\infty}p(n_1,n_2). \tag{87}$$

Solid curves in Fig. 10 show the photon number distribution $p_1(n_1)$ of mode 1 as a function of n_1 for different values of σ/n_o. Below threshold ($\sigma/n_o<1$), the peak of the distribution is at zero. As σ/n_o increases from below to above threshold, the peak of the distribution gradually moves to the right to nonzero values of n_1. This behavior of $p_1(n_1)$ is similar to the photon number distribution for the single-mode laser [16].

Another quantity of interest is the PND variable $n=n_1-n_2$. We expect this variable to vanish in the mean since photons are created in pairs inside the cavity. Indeed, it can be seen that $p(n_1,n_2)$ is an even function of n_1-n_2. However, once inside the cavity, photons from each pair can escape independently causing photon number difference to fluctuate. These fluctuations also exhibit nonclassical features. We can obtain the distribution for the photon number difference variable $n\equiv n_1-n_2$ by introducing two independent variables

$$n=n_1-n_2, \quad -\infty<n<\infty,$$

$$N=n_1+n_2, \quad |n|\le N<\infty. \tag{88}$$

Expressing $p(n_1,n_2)$ in terms of these variables and summing over N, with a simple change of variable $s=N-|n|$ ($0\le s<\infty$), we obtain the distribution for the PND variable n,

$$\wp_n=\frac{1}{Z}\sum_{s=0}^{\infty}\sum_{m=0}^{\infty}\frac{(\sigma/2)^{2m+2s+2|n|}}{s!\,(s+|n|)!\,m!\,(m+|n|)!}\left[\frac{\Gamma(m+s+|n|+1)!\,\Gamma(n_o)}{\Gamma(n_o+m+s+|n|+1)}\right]^2. \tag{89}$$

This distribution depends only on the absolute value of n and guarantees that all normally ordered odd-order moments of n including the mean vanish.

Below threshold ($\sigma/n_o<1$), the joint photon number distribution can be evaluated in terms of a hypergeometric function. The resulting expression, however, is not very illuminating and will not be reproduced here. On the other hand, the distribution of photon number difference variable $n=n_1-n_2$ below threshold takes the form of a geometric distribution given by

$$\wp_n\approx\left[\frac{1-\beta^2+\sqrt{1-\beta^2}}{1+\sqrt{1-\beta^2}}\right]\left(\frac{\beta^2}{2-\beta^2+2\sqrt{1-\beta^2}}\right)^{|n|}, \quad \beta=\frac{\sigma}{n_o}. \tag{90}$$

This below threshold result is an excellent approximation to the exact result (89) even very close to threshold ($\sigma/n_o\le 0.99$) for n_o as small as $\approx 10^4$. For larger n_o, the agreement improves for operating points even closer to threshold. The distribution $\wp_n$ [Eq. (89)] for the photon difference variable is shown in Fig. 11 for several values of σ/n_o from below to

above threshold. Below threshold ($\sigma/n_o=0.995$), the results from Eq. (90) are indistinguishable from the exact results in Fig. 11.

As already noted following Eq. (89), all normally ordered moments of odd powers of $n=n_1-n_2$ vanish. For normally ordered even-order moments of n, we find

$$\langle:(\Delta\hat{n})^{2r}:\rangle = \left(\frac{(-)^r(2r-1)!!}{2^r}\right)\sum_{m=0}^{\infty}\frac{(m+r)!}{m!}\frac{\sigma^{2(m+r)}}{[\Gamma(m+r+n_o+1)]^2}\Big/\sum_{m=0}^{\infty}\frac{\sigma^{2m}}{[\Gamma(m+n_o+1)]^2}. \tag{91}$$

Note that even-order moments of n for $r=2,4,6,\ldots$ are positive quantities whereas those for $r=1,3,5,\ldots$ are negative quantities. The negative values of the latter set of moments are a reflection of the nonclassical character of light from the NDPO and is a direct consequence of cross correlation between down-converted modes being stronger than autocorrelations [18,37].

IV. CONCLUSION

In this paper, we have discussed the quantum statistical properties of light emitted by degenerate and nondegenerate parametric oscillators in the region of threshold. Unlike the regions far below and above threshold where one can linearize the equations of motion around the steady states, near threshold one must take full account of the nonlinearity of mode-mode interaction. By using positive-P phase-space representation of the density matrix of the field, we were able to derive a Fokker-Planck equation for the positive-P function and its steady-state solution that takes into account the full nonlinearity of the problem as well as the quantum-mechanical nature of the noise. The steady-state solution allows us to derive analytic expressions for various quantities such as the mean, variance, and higher-order moments of photon number variables. With the help of these expressions, we are able to provide a quantitative description of the transformation that the fluctuations undergo in passing the threshold. We find that most dramatic changes occur in a very narrow range given, approximately, by $|\sigma/n_o-1|\leq 10/\sqrt{n_o}$. Although the transformation of many quantities as the OPO passes its threshold mirrors, the transformation of corresponding quantities for the single- and two-mode lasers, there are important differences. In particular, the light from the OPO retains many of its nonclassical characteristics even as it undergoes this transformation. It is remarkable that the steady-state expressions presented here for various quantities pertaining to the OPO not only describe the threshold transformation but also encompass the inherently nonclassical character of light produced by these oscillators.

The results obtained by using the simpler distributions presented here are in excellent agreement with those obtained from the exact distributions for large values of n_o. This is the regime in which most laboratory OPOs currently operate. These simpler distributions allow us to investigate properties of the OPOs in an analytic fashion and provide simple intuitive picture of their fluctuation properties. For systems with small values of n_o, the approximations we have may become suspect. A similar analytic description of the OPOs in this limit will require further exploration and different types of approximations. However, in this limit, we can always revert to the exact distribution $p(\vec{x})$ given in this paper to discuss the fluctuation properties of OPOs.

[1] R. Loudon and P. L. Knight, special issue of J. Mod. Opt. **34**, 709 (1987); P. W. Milonni and S. Singh, in *Advances in Atomic, Molecular, and Optical Physics*, edited by D. Bates and B. Bederson (Academic, Orlando, FL, 1991), Vol. 28, pp. 75–142.

[2] L. A. Wu, H. J. Kimble, J. L. Hall, and H. Wu, Phys. Rev. Lett. **57**, 2520 (1986).

[3] A. Heidmann, R. J. Horowicz, S. Reynaud, E. Giacobino, C. Fabre, and G. Camy, Phys. Rev. Lett. **59**, 2555 (1987).

[4] X. L. Su, A. Tan, X. J. Jia, Q. Pan, C. D. Xie, and K. C. Peng, Opt. Lett. **31**, 1133 (2006).

[5] A. S. Villar, L. S. Cruz, K. N. Cassemiro, M. Martinelli, and P. Nussenzveig, Phys. Rev. Lett. **95**, 243603 (2005).

[6] J. Jing, S. Feng, R. Bloomer, and O. Pfister, Phys. Rev. A **74**, 041804(R) (2006).

[7] O. Aytur and P. Kumar, Phys. Rev. Lett. **65**, 1551 (1990).

[8] D. T. Smithey, M. Beck, M. Belsley, and M. G. Raymer, Phys. Rev. Lett. **69**, 2650 (1992).

[9] Y. J. Lu and Z. Y. Ou, Phys. Rev. Lett. **88**, 023601 (2001).

[10] E. Waks, E. Diamanti, B. C. Sanders, S. D. Bartlett, and Y. Yamamoto, Phys. Rev. Lett. **92**, 113602 (2004).

[11] A. Zavatta, S. Viciani, and M. Bellini, Phys. Rev. A **72**, 023820 (2005).

[12] V. D'Auria, S. Fornaro, A. Porzio, S. Solimeno, S. Olivares, and M. G. A. Paris, Phys. Rev. Lett. **102**, 020502 (2009).

[13] R. Vyas and S. Singh, Phys. Rev. A **38**, 2423 (1988); Opt. Lett. **14**, 1110 (1989); Phys. Rev. A **40**, 5147 (1989); R. Vyas and A. L. DeBrito, *ibid.* **42**, 592 (1990).

[14] M. J. Wolinsky and H. J. Carmichael, Phys. Rev. Lett. **60**, 1836 (1988); H. J. Carmichael, *An Open Systems Approach to Quantum Optics* (Springer-Verlag, Berlin, 1993).

[15] G. S. Agarwal and G. Adam, Phys. Rev. A **39**, 6259 (1989).

[16] L. Mandel and E. Wolf, *Optical Coherence and Quantum Optics* (Cambridge University Press, New York, 1995), Chap. 18 and 19.

[17] S. Singh, Phys. Rep. **108**, 217 (1984).

[18] R. Vyas and S. Singh, Phys. Rev. Lett. **74**, 2208 (1995).
[19] C. K. Hong, Z. Y. Ou, and L. Mandel, Phys. Rev. Lett. **59**, 2044 (1987).
[20] T. Kim, O. Pfister, M. J. Holland, J. Noh, and J. L. Hall, Phys. Rev. A **57**, 4004 (1998).
[21] R. A. Campos, B. E. A. Saleh, and M. C. Teich, Phys. Rev. A **40**, 1371 (1989).
[22] P. D. Drummond and C. W. Gardiner, J. Phys. A **13**, 2353 (1980).
[23] M. D. Reid and L. Krippner, Phys. Rev. A **47**, 552 (1993).
[24] P. D. Drummond and M. D. Reid, Phys. Rev. A **41**, 3930 (1990).
[25] R. Vyas, Phys. Rev. A **46**, 395 (1992).
[26] R. Vyas and S. Singh, Phys. Rev. A **62**, 033803 (2000).
[27] H. Deng, D. Erenso, R. Vyas, and S. Singh, Phys. Rev. Lett. **86**, 2770 (2001).
[28] S. Siddiqui, D. Erenso, R. Vyas, and S. Singh, Phys. Rev. A **67**, 063808 (2003); J. Vines, R. Vyas, and S. Singh, *ibid.* **74**, 023817 (2006).
[29] P. D. Drummond, K. J. McNeil, and D. F. Walls, Opt. Acta **27**, 321 (1980); **28**, 211 (1981).
[30] A. B. Dodson and R. Vyas, Phys. Rev. A **47**, 3396 (1993); R. Vyas and S. Singh, J. Opt. Soc. Am. B **17**, 634 (2000).
[31] S. Chaturvedi, K. Dechoum, and P. D. Drummond, Phys. Rev. A **65**, 033805 (2002); P. D. Drummond, K. Dechoum, and S. Chaturvedi, *ibid.* **65**, 033806 (2002).
[32] K. J. McNeil and C. W. Gardiner, Phys. Rev. A **28**, 1560 (1983).
[33] W. Magnus, F. Oberhettinger, and R. P. Soni, *Formulas and Theorems for the Special Functions of Mathematical Physics* (Springer-Verlag, New York, 1966).
[34] M. M-Tehrani and L. Mandel, Phys. Rev. A **17**, 694 (1978).
[35] S. Singh and L. Mandel, Phys. Rev. A **20**, 2459 (1979); S. Singh, Opt. Commun. **32**, 339 (1980).
[36] H. J. Carmichael, *An Open Systems Approach to Quantum Optics*, Lecture Notes in Physics Vol. 18 (Springer-Verlag, Berlin, 1993); *Statistical Methods in Quantum Optics 2: Non-Classical Fields* (Springer-Verlag, Berlin, 2008).
[37] L. Mandel, Phys. Scr. **T12**, 34 (1986).